








Impedance Modeling of Common Mode Ferrite Chokes Using Transmission Line Theory

Alejandro Muñoz Manterola , Luis Manuel Diaz Angulo , *Member, IEEE*, Alberto Gascón Bravo , Kenan Tekbaş , María Tijero , Roberto Moreno , and Salvador G. Garcia , *Senior Member, IEEE*

Abstract—An impedance model, based on transmission line theory, is introduced for common mode ferrite chokes. The proposed model takes into account the geometrical properties of the choke, the distribution of electromagnetic fields within the core material and the impact of the measurement setup. The validity of the model was tested through numerical simulations. As a practical application, the model was applied to estimate the complex permeability of manganese zinc (MnZn) and nickel zinc (NiZn) cores from impedance measurements, resulting in a range of values compatible with those reported in other works.

Index Terms—Mn-Zn ferrite, Ni-Zn ferrite, complex permeability, ferrite core modeling, finite element method (FEM), transmission lines (TLs).

I. INTRODUCTION

COMMON mode (CM) chokes are widely used components in both industrial and laboratory applications to filter high-frequency (HF) CM currents [1]. In the case of semiconductor converters, the conducted and radiated emissions induced by the HF currents can generate some harmonics up to 400 MHz [2]. From the electromagnetic immunity perspective, the energy coming from other circuits or from the outside of the equipment could also have some ultra-HF components that should be filtered as well. The performance of chokes to filter out these unwanted HF signals is usually governed by their impedance characteristics. However, the characterization of CM chokes can

be challenging due to the influence of multiple factors, such as the core's material composition, its geometric dimensions, the measurement setup and the operating frequency. The modeling of the choke's impedance has to take into account that ferrites can have, simultaneously, both a large permeability and a permittivity, leading to an inhomogeneity of the fields inside the ferrite [3], [4], [5], [6]. This effect has to be properly modeled to yield precise results. In an analogous way, the extraction of physical parameters from impedance measurements has to consider the previous factor, and the influence of the measurement setup at high frequencies. Otherwise, those effects will be included in the frequency dependence of the ferrite parameters, and one might find different physical properties for ferrites made of the same material [7].

The most common approach to model the impedance of CM chokes is to use a circuit composed of a series inductor–resistor in parallel with a capacitor element [8], [9]. CM chokes commonly show an HF peak impedance [10], which in these models is interpreted as an LC resonance. From this resonance, a capacitance is computed to make it coincide with the measured peak. Although this approach is simple and effective in capturing the main features of the impedance behavior at low frequencies and does predict a peak in impedance it fails to predict the frequency dependence of the impedance at HF. Moreover, the capacitance value obtained to position the peak is difficult to justify from a physical point of view. This capacitance is typically attributed to the wire winding [11]. Nevertheless, this explanation does not hold for chokes with either one turn of wire as typical CM chokes or even none at all, as in the case of beads.

In the context of transformers and inductors, some impedance models account for core losses through a complex magnetic permeability and a complex electric permittivity, which are assumed to be known [12], [13]. When the complex permeability is accounted for, these models are able to predict the frequency dependence of the impedance and have the merit of weighting the influence of the winding resistances on the total impedance. However, these models still cannot predict the observed impedance peaks from geometric or material properties, which are still attributed to inter or intra-winding capacitances.

Other approaches have focused on characterizing the complex permeability of ferrite materials by measuring the impedance of a solenoid that uses them as a core [14], [15], [16], [17]. For some types of ferrites, e.g., manganese zinc (MnZn), these models are able to properly predict the frequency dependence of the impedance. However, for other materials, such as nickel

Manuscript received 28 September 2023; revised 15 November 2023; accepted 8 December 2023. Date of publication 8 January 2024; date of current version 16 February 2024. This work was supported in part by the Spanish National Project under Grant PID2022-137495OB-C31 (ESAMA), in part by European project HECATE, in part by Spanish MICINN EU FEDER Project under Grant PID2019.106120RB.C33, in part by EU Horizon2020 Research and Innovation Programme under the Marie Skłodowska-Curie Action under Grant 101066571, and in part by Junta de Andalucía FEDER Project B-TIC-700-UGR20. Recommended for publication by Associate Editor W. Huang. (Corresponding author: Luis Manuel Diaz Angulo.)

Alejandro Muñoz Manterola, Luis Manuel Diaz Angulo, Alberto Gascón Bravo, and Salvador G. Garcia are with the Department of Electromagnetism, University of Granada, 18071 Granada, Spain (e-mail: almuma@ugr.es; lmdi-azangulo@ugr.es; agascon@ugr.es; salva@ugr.es).

Kenan Tekbaş is with the Department of Electromagnetism, University of Granada, 18071 Granada, Spain, and also with the Department of Electrical and Electronic Engineering, Amasya University, Amasya 05100, Türkiye (e-mail: kenan.tekbas@ugr.es).

María Tijero and Roberto Moreno are with IKERLAN Technology Research Centre, Basque Research and Technology Alliance (BRTA), 20500 Arrasate/Mondragón, Spain (e-mail: mtijero@ikerlan.es; rmoreno@ikerlan.es).

Color versions of one or more figures in this article are available at <https://doi.org/10.1109/TPEL.2023.3343504>.

Digital Object Identifier 10.1109/TPEL.2023.3343504

zinc (NiZn), the impedance do not match the data well, and there is discrepancy between different applications of the model: the authors in [7], [18], [19], and [16] reported frequency behaviors, which are not mutually compatible. Additionally, these models assume that the field distribution inside the ferrite is homogeneous, which is not always the case when the ferrites have air gaps or cracks on the surface or volume, or when the effect of the skin depth is taken into account. This assumption also leads to different permeability values for ferrites of the same material.

The electric conductivity of ferrite materials has also been studied, and it has been shown to increase with frequency in [7], [17], [19], [20], [21], [22]. This can result in a significant skin effect, which causes a nonhomogeneous field distribution inside the material. To avoid these effects, in [19], ferrites that are only a few millimeters in size were used, where the skin and wavelength effects are considered negligible. Although this technique accurately removes the dimensional effects for the complex permeability measurements, it requires the capability of manufacturing ferrite cores specifically for this purpose, thus introducing variability and making it hard to evaluate commercially available cores.

To mitigate these limitations, we propose a method in Section II to calculate the impedance of the CM ferrite choke, based on transmission line (TL) analysis, which considers the possible inhomogeneity of the fields due to skin depth effects, geometrical characteristics, and the impact of the measurement setup. The proposed model aims to accurately represent the main features of the measured impedance, namely the slope variations and the resonance peaks. The parameters in the model are solely derived from physical considerations and do not require an a posteriori capacitance estimation. In Section III, we validate the model by comparing its impedance predictions with FEM-based simulations and experimental data.

II. IMPEDANCE MODEL DERIVATION USING TL THEORY

A. Modeling of CM Choke as a TL

Let us consider a ferrite choke with an internal radius r_i , a thickness d_m , a width of l_m , an average internal circumference w , and wound with a single turn of wire having a total length of $2l + d$, as shown in Fig. 1. Our goal is to determine the impedance Z_{in} , which would be measured at the terminals of the wire. Hence, we will use a TL analogy for the derivation of impedance model, in which the conductors of the TL have length l and separated by a distance d and ending in a short. We assumed that a portion of the TL is filled with the material which constitutes the choke with the permittivity, ϵ_m , and the permeability, μ_m and the remaining space is vacuum with ϵ_0 , and μ_0 .

At any point z of the TL, the voltage between the conductors $V(z)$ is given by the Heaviside's equations as [23]

$$\frac{d^2 V(z)}{dz^2} - \gamma_{TL}^2 V(z) = 0 \quad (1a)$$

$$\frac{d^2 I(z)}{dz^2} - \gamma_{TL}^2 I(z) = 0 \quad (1b)$$

where γ_{TL} is the complex propagation constant of the TL.

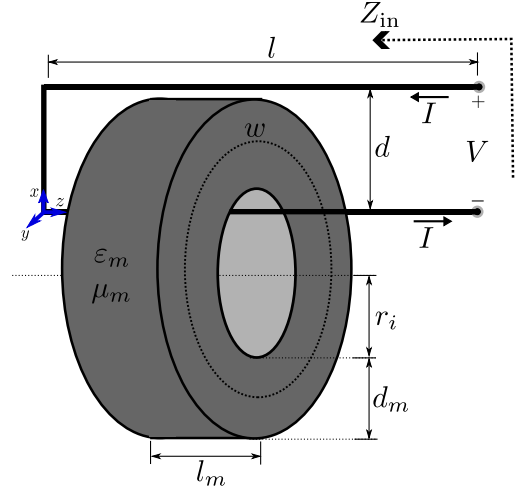


Fig. 1. Schematic representation of a ferrite choke wound with a single wire turn. The TL is formed by the bent wire and terminated in a short circuit.

The input impedance Z_{in} presented by a homogeneous TL of length l , with characteristic impedance Z_{TL} and terminated with a load Z_L is given by

$$Z_{in} = Z_{TL} \frac{Z_L + Z_{TL} \tanh(\gamma_{TL} l)}{Z_{TL} + Z_L \tanh(\gamma_{TL} l)}. \quad (2)$$

If the line is not homogeneous, its parameters will depend on the specific position along the line z , i.e., $Z_{TL}(z)$ and $\gamma_{TL}(z)$. Discretizing the space in z_i points with $i = 1, \dots, N$, Z_{in} at any point $z_i = z_{i+1} - \Delta z$ of the TL can be obtained using a recursive formula

$$Z_{in}(z_i) = Z_{TL} \frac{Z_{in}(z_{i+1}) + Z_{TL}(z_{i+1}) \tanh(\gamma_{TL}(z_{i+1}) \Delta z)}{Z_{TL}(z_{i+1}) + Z_{in}(z_{i+1}) \tanh(\gamma_{TL}(z_{i+1}) \Delta z)} \quad (3)$$

where Δz and $Z_{TL}(\Delta z)$ are, respectively, the length and the impedance of the slice of material that is being incorporated into the input impedance, and $Z_{in}(z_{i+1})$ is the input impedance computed in the previous step. The end of the line can be considered short-circuited ($Z_L = 0$) or can include the load caused by the experimental setup using standard TL considerations. To utilize (3) for the impedance calculation of the choke, we need to determine the TL parameters, γ_{TL} and Z_{TL} .

B. Derivation of TL Parameters

To obtain the TL parameters γ_{TL} and Z_{TL} , we need to establish a relationship between V and I in the wire. This relationship can be established by integrating the electric and magnetic fields (\mathbf{E} and \mathbf{H}) between the conductors. Therefore, our first step is to derive the expressions for these fields. Let us properly define this problem using Maxwell's equations in the frequency domain

$$\nabla \times \mathbf{E} = -j\omega\mu\mathbf{H} \quad (4a)$$

$$\nabla \times \mathbf{H} = j\omega\epsilon\mathbf{E} \quad (4b)$$

where the effective permittivity has the general form

$$\epsilon(\omega) = \epsilon' - j\epsilon'' \quad (5)$$

and the effective permeability

$$\mu(\omega) = \mu' - j\mu'' \quad (6)$$

both being complex-valued and frequency dependent quantities. Equations (4)–(6) can be combined to derive Helmholtz's equation

$$\nabla^2 \mathbf{E} = \gamma^2 \mathbf{E} \quad (7a)$$

$$\nabla^2 \mathbf{H} = \gamma^2 \mathbf{H} \quad (7b)$$

where

$$\gamma = jk = \alpha + j\beta \quad (7c)$$

being the complex propagation constant, $k = \omega\sqrt{\varepsilon\mu}$ the complex wavenumber, α the attenuation constant, and β the phase constant or wavenumber [23]. The complex propagation constant γ describes how the fields evolve within the cross-section of our TL, this is a different quantity to the γ_{TL} defined in (1), which defines how the voltage and currents propagate along the TL. Moreover, γ is a property of materials, which depends on their specific ε and μ , while γ_{TL} depends on the composition of the cross-section, which may include more than one material in general.

For our specific problem, (7) can be solved for toroidal geometries using Bessel's equation and cylindrical coordinates [12], [24]. However, if we assume a large internal radius, (7) can be formulated in Cartesian coordinates as

$$(\partial_x^2 + \partial_z^2)\mathbf{E} = \gamma_i^2 \mathbf{E} \quad (8a)$$

$$(\partial_x^2 + \partial_z^2)\mathbf{H} = \gamma_i^2 \mathbf{H} \quad (8b)$$

with subscripts $i = \{0, m\}$ for the free space or the ferrite material, respectively. The contour conditions can also be derived from the surface current density, \mathbf{J}_s , and the surface charge density, ρ_s , at the conductor surfaces as

$$\mathbf{E}_0 \cdot \hat{\mathbf{n}} = \frac{\rho_s}{\varepsilon} \quad (9a)$$

$$\mathbf{H}_0 \times \hat{\mathbf{n}} = \mathbf{J}_s \quad (9b)$$

which is equivalent to the formulation of the problem in Cartesian coordinates with symmetry along the y -axis (see Fig. 2). Hence, we assume that the current $I(z)$ and charge $Q(z)$ are distributed uniformly along the y -axis on a surface that embraces the toroid's upper, lower, and internal faces.

1) *Homogeneous Field Along z -Axis Approach:* To simplify the problem, let us first assume that the thickness l_m of the ferrite is much longer than its height d_m . This approach allows us to assume a uniform field distribution along the TL as shown in Fig. 2(a), i.e., the fields do not depend on the position along the z -direction. Thus, (8) reduces to

$$d_x^2 E_x = \gamma_i^2 E_x \quad (10a)$$

$$d_x^2 H_y = \gamma_i^2 H_y. \quad (10b)$$

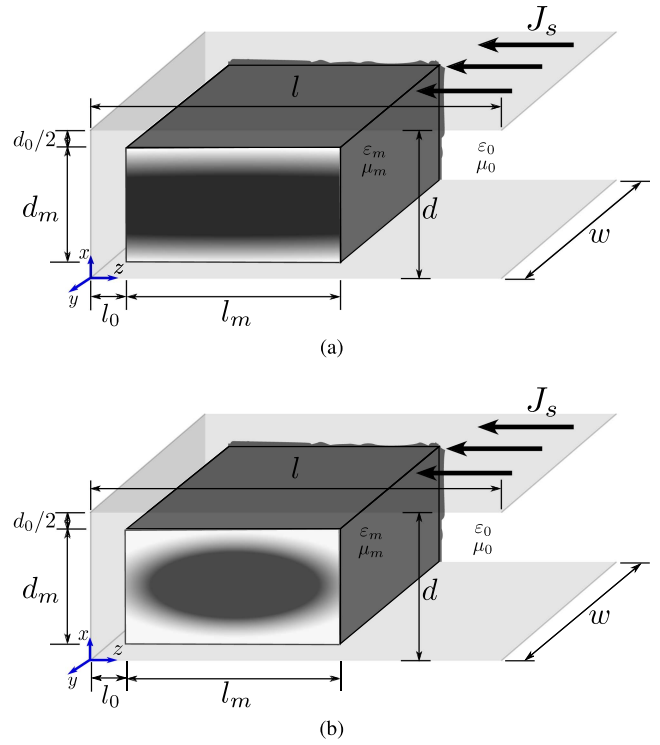


Fig. 2. Ferrite choke as a TL with the approximations of field distribution. (a) Homogeneous field along the z -axis assumes $l_m \gg d_m$. (b) Inhomogeneous field along the z -axis assumes $l_m \sim d_m$. Lighter colors represent a higher intensity of \mathbf{E} and \mathbf{H} fields.

Considering $d_0 + d_m = d$, with d being the distance between wires, (10a) can be solved as

$$E_x(x) = \begin{cases} E_{x,0} & x \in x_0 \\ E_{x,m} \frac{\cosh(\gamma_m(x-d_0/2-d_m/2))}{\cosh(\gamma_m d_m/2)} & x \in x_m \end{cases} \quad (11)$$

where x_0 and x_m correspond to the regions along the x -axis in free space and filled the ferrite material, respectively. Here, we consider $\gamma_0 \ll \gamma_m$, a valid assumption for typical problems, and use the continuity equation at the boundary between free space and the ferrite as

$$E_{x,0} \varepsilon_0 = E_{x,m} \varepsilon_m \quad (12)$$

and relate the charge in the conductor at $x = 0$ to the normal electric field as

$$E_{x,0} = \frac{\rho_s}{\Delta z \varepsilon_0} = \frac{Q}{w \Delta z \varepsilon_0} \quad (13)$$

where w is the distance along the y -axis in which the ρ_s and \mathbf{J}_s are present. In our case, $w = 2\pi r$, with r being the distance to the toroidal center; therefore, w depends on z , and we can no longer talk about a homogeneous field. To avoid this complexity, we will perform the computation using an average radius, which allows us to consider w as constant. We can now use (11) to compute the voltage between the two conductors at a specific point z in the line, which can be written as

$$V = - \int_d^0 \mathbf{E} \cdot \hat{\mathbf{x}} dx$$

$$\begin{aligned}
 &= Q \left(\frac{d_0}{\Delta z w \varepsilon_0} + \frac{1}{\Delta z w \varepsilon_m} \frac{2 \tanh(\gamma_m d_m/2)}{\gamma_m} \right) \\
 &= Q (\Delta z C_0^{-1} + \Delta z C_m^{-1}) \\
 &= Q \Delta z \tilde{C}^{-1}
 \end{aligned} \tag{14}$$

where we denote \tilde{C} as a complex capacitance per unit length of the line, with separate contributions from the air gap (C_0) and the ferrite material (C_m).

The magnetic field in (10b) has the same formal solution as (11)

$$H_y(x) = \begin{cases} H_{y,0} & x \in x_0 \\ H_{y,m} \frac{\cosh(\gamma_m(x-d_0/2-d_m/2))}{\cosh(\gamma_m d_m/2)} & x \in x_m \end{cases} \tag{15}$$

and

$$H_{y,0} = H_{y,m}. \tag{16}$$

The current I in the conductor at $x = 0$ allows us to calculate the tangential magnetic field as

$$H_{y,0} = J_{s,z} = -\frac{I}{w} \tag{17}$$

and the magnetic flux ϕ_B on xz section S

$$\begin{aligned}
 \phi_B &= \iint_S \mathbf{B} \cdot \hat{\mathbf{y}} dS \\
 &= I \left(\Delta z \mu_0 \frac{d_0}{w} + \Delta z \mu_m \frac{1}{w} \frac{2 \tanh(\gamma_m d_m/2)}{\gamma_m} \right) \\
 &= I (\Delta z L_0 + \Delta z L_m) \\
 &= I \Delta z \tilde{L}
 \end{aligned} \tag{18}$$

where we can identify \tilde{L} as a complex inductance per unit length, with contributions from the air gap (L_0) and from the ferrite material (L_m). Finally, we can use Faraday's law on the same surface to obtain

$$\int_{\partial S} \mathbf{E} \cdot d\mathbf{l} = -j\omega \phi_B \tag{19}$$

from which we can deduce, in the limit $\Delta z \rightarrow 0$

$$\partial_z V(z) = -j\omega \tilde{L} I(z). \tag{20}$$

Using the charge continuity equation on the upper conductor volume V and integrating on the boundary of V , we can define

$$\int_{\partial V} \mathbf{J} \cdot d\mathbf{S} = -j\omega Q(z) \tag{21}$$

which in the same limit allows us to write

$$\partial_z I(z) = j\omega \tilde{C} V(z). \tag{22}$$

By inserting (22) into (20), we can deduce the complex propagation constant, which appears in (1) as

$$\gamma_{TL} = j\omega \sqrt{\tilde{L}\tilde{C}} \tag{23}$$

and

$$Z_{TL} = \sqrt{\frac{\tilde{L}}{\tilde{C}}}. \tag{24}$$

It should be noted that these terms are similar to those used in lossless TLs, where $Z_0 = \sqrt{L/C}$. However, the losses and dispersion are present in our scenario since \tilde{L} and \tilde{C} are complex numbers.

2) *Inhomogeneous Field Approach*: With the insights gained from the previous approach, we can now aim to solve the problem posed in (8) for the case in which $d_m \sim l_m$ [see Fig. 2(b)]. Outside the ferrite material, for typical dimensions, the solution of (8) can be considered constant as $\gamma_0 \ll \gamma_m$. Inside the ferrite material, a more general analytical solution for the field can be found in [25]

$$\begin{aligned}
 \mathbf{H}(x, z) &= \mathbf{H}_0 \left[\frac{\cosh(\gamma_m z)}{\cosh(\gamma_m b)} \right. \\
 &\quad \left. + \sum_{n \text{ odd}} c_n \cos\left(\frac{n\pi z}{2b}\right) \cosh\left(x \sqrt{\gamma_m^2 + \frac{n^2 \pi^2}{4b^2}}\right) \right]
 \end{aligned} \tag{25}$$

with

$$c_n = \frac{4\gamma_m^2}{n\pi} \sin\frac{n\pi}{2} \frac{1}{\gamma_m^2 + \frac{n^2 \pi^2}{4b^2} \cosh\left(a \sqrt{\gamma_m^2 + \frac{n^2 \pi^2}{4b^2}}\right)} \tag{26}$$

where $a = d_m/2$ and $b = l_m/2$. The main consequence of this added complexity is that now the complex inductance L_m depends on the position z . Despite that, we can operate similarly to obtain

$$\begin{aligned}
 L_m(z) &= \int_{-a}^a H(x, z) dx \\
 &= \frac{\mu}{2\pi r_{av}} \left[\frac{2 \tanh(\gamma_m b)}{\gamma_m} \right. \\
 &\quad \left. + \sum_{n \text{ odd}} c'_n \cosh\left(z \sqrt{\gamma_m^2 + \left(\frac{n\pi}{2b}\right)^2}\right) \right]
 \end{aligned} \tag{27}$$

with

$$c'_n = \frac{16\gamma_m^2 b}{n^2 \pi^2} \frac{1}{\gamma_m^2 + \left(\frac{n\pi}{2b}\right)^2} \frac{1}{\cosh\left(a \sqrt{\gamma_m^2 + \left(\frac{n\pi}{2b}\right)^2}\right)}. \tag{28}$$

From the discussion carried out in Section II-B1, we know that for a typical problem $L_0 \ll L_m$ and $C_0 \ll C_m$, therefore

$$\tilde{L} \simeq L_m \tag{29a}$$

$$\tilde{C} \simeq C_0 \tag{29b}$$

which allow us to model the ferrite as a distributed component with the equivalent circuit parameters (\tilde{L} and \tilde{C}) as shown in Fig. 3 and compute γ_{TL} , Z_{TL} , and Z_{in} from (23), (24), and (3), respectively.

III. VALIDATION OF THE MODEL

A. Comparison With Numerical Simulations

In this section, we aim to determine the accuracy of the proposed TL impedance model. To do this, we will assume a

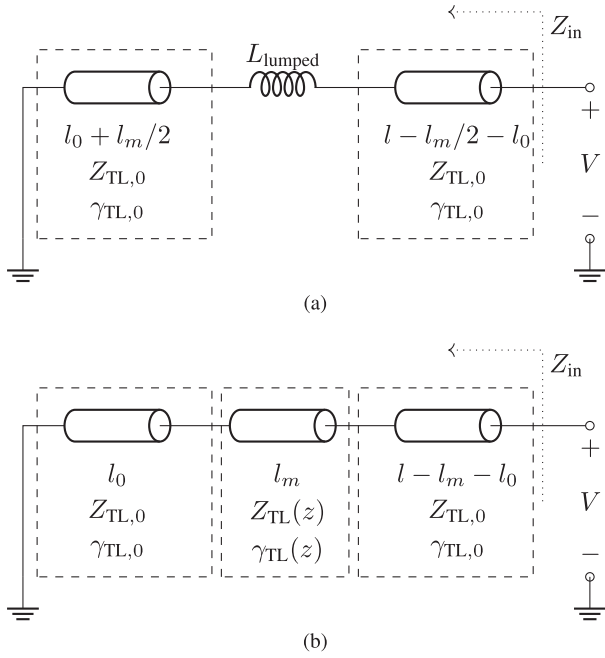


Fig. 3. Different models employed to obtain input impedance. (a) Lumped element impedance calculation. (b) TL impedance model proposed.

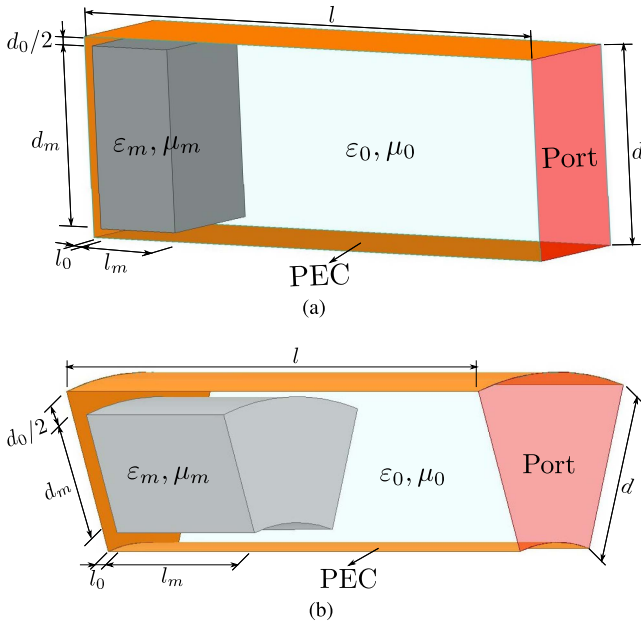


Fig. 4. Geometrical setups used, showing dimensions and boundary conditions used to perform FEM simulations. (a) Cartesian setup. (b) Coaxial setup.

fictitious ferrite material with effective material constants

$$\mu_m = \mu_{m,r} \mu_0 \quad (30a)$$

$$\epsilon_m = \epsilon_0 - j\sigma_m/\omega \quad (30b)$$

with $\mu_{m,r} = 620$ and $\sigma = 5 \text{ S/m}$. Two different setups have been used. The Cartesian setup [see Fig. 4(a)] has translational symmetry and fits better the assumptions made to derive (27); thus, we would expect to obtain a better agreement with this

setup. The coaxial setup [see Fig. 4(b)] employs cylindrical symmetry of the fields around a toroidal ferrite, and is a typical configuration when the aim is to characterize the properties of a ferrite [26]. Using (7c) and the values in (30), we can compute the skin depth and wavelength in the ferrite core and note that they are comparable to the size of the ferrite for most of the range of frequency studied, e.g., at 100 MHz, the skin depth is $\delta = \alpha^{-1} \sim 0.9 \text{ mm}$ and the wavelength is $\lambda = 2\pi\beta^{-1} \sim 5.7 \text{ mm}$, comparable to the dimensions of the setup. Therefore, we can expect to have a significant field inhomogeneity and the resonant effects reported in [3] and [4], a challenging test for most impedance models.

To evaluate the validity of our approach, we will compare the results obtained with our theoretical models and the ones obtained with a frequency domain finite element method (FEM) solver (*Ansys high frequency structure simulator (HFSS)*). To do this, the Cartesian and coaxial setups were modeled as shown in Fig. 4. We used perfect electric conductor boundaries for all the metallic surfaces and perfect magnetic conductor boundaries to model symmetry boundary conditions. A current was introduced between the extremes of the conductors using a lumped source. The dimensional parameters of Cartesian setup in Fig. 4(a) are $d_m = 20 \text{ mm}$, $d_0 = 2 \text{ mm}$, $d = 22 \text{ mm}$, $l_m = 10 \text{ mm}$, $l_0 = 1 \text{ mm}$, and $l = 60 \text{ mm}$, whereas the parameters of Coaxial setup in Fig. 4(b) are $d_m = 12.75 \text{ mm}$, $d_0 = 4 \text{ mm}$, $d = 16.75 \text{ mm}$, $l_m = 20 \text{ mm}$, $l_0 = 2 \text{ mm}$, and $l = 60 \text{ mm}$.

We used two impedance models to compute the impedance, with equivalent electric circuits shown in Fig. 3. The lumped element impedance model [see Fig. 3(a)], assumes that the ferrite can be modeled by a lumped inductance calculated using (27) as

$$L_{\text{lumped}} = \sum_{i=1}^N L_m(z_i) \quad (31)$$

with $l = N\Delta z$ and $z_i = (i-1)\Delta z + \Delta z/2$, with $N = 201$. In this model, L_{lumped} is put in series with two TL segments, which account for the distances between the source and the short-circuit load at the end of the setup. The characteristic impedance and complex propagation constant of these segments, $Z_{\text{TL},0}$ and $\gamma_{\text{TL},0}$ can be obtained by standard procedures [23] being, for the Cartesian setup

$$Z_{\text{TL},0} = \sqrt{\frac{\mu_0}{\epsilon_0}} \frac{d}{w} \quad (32)$$

with $w = 151.6 \text{ mm}$. For the Coaxial setup

$$Z_{\text{TL},0} = \sqrt{\frac{\mu_0}{\epsilon_0}} \frac{\log(r_o/r_i)}{2\pi} \quad (33)$$

with $r_i = 17.75 \text{ mm}$ and $r_o = 30.5 \text{ mm}$, the same dimensions as one of the cases, which will be later addressed in Section III-B. For both cases $\gamma_{\text{TL},0} = j\omega\sqrt{\mu_0\epsilon_0}$. In the TL impedance model [see Fig. 3(b)], the lumped impedance is substituted by an inhomogeneous TL with $Z_{\text{TL}}(z)$ and $\gamma_{\text{TL}}(z)$ given by (23) and (24) and using (3) to derive the input impedance, which would be measured.

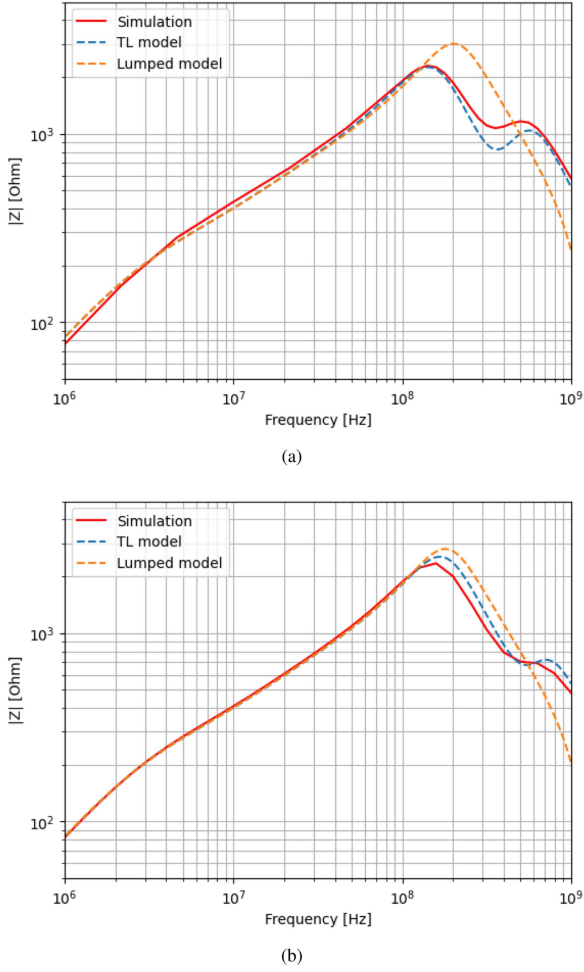


Fig. 5. Impedance results (a) Cartesian and (b) Coaxial with an FEM simulation (red), the proposed TL model (blue) and a lumped inductance calculation (orange). The simulation data have been considered as the reference solution.

The results for the simulations and the evaluated models are presented in Fig. 5 for the two geometries studied. Below the resonance peak, both geometries and both models make almost identical predictions; below 2 MHz both have the +20 dB/dec slope, which characterizes ideal inductors. We can observe a $\sim +10$ dB/dec up to 100 MHz, which is characteristic of the skin depth effect, because the field is no longer homogeneous and constant inside the choke. This is a similar result to what can be obtained with other models, such as the ones in [12] and [24]. However, we observe differences between the models at higher frequencies, there is a second resonance peak, which the lumped model fails to predict. This mode is caused by a resonance, which depends on the specific characteristics of the setup and the dimensions of the choke and that a pure lumped model cannot reproduce. On the other hand, the TL impedance model accounts for the speed of the voltage wave as it travels through the wire, and we can observe that its predictions match much better the reference solution at high frequencies. It is also worth noting that both models show good agreement for the two geometries studied, which used different assumptions with respect to symmetry. This indicates that neglecting the radial dependency in Bessel's equation made in Section II was a good assumption to model these cases.

B. Parameter Extraction

In the previous section, we assumed that the electromagnetic properties were known a priori and used them as inputs for the developed model to make impedance predictions. In this section, as an additional validation and as an application example, we will solve the *inverse problem*, i.e., the deduction of the effective permeability μ_m and permittivity ε_m parameters of a CM choke from its impedance measurements using different experimental setups. To accomplish this, we will use an optimization procedure to find the parameters, which produce the best match with the experimental measurements.

The impedance of the TL (24), through its dependence on \tilde{L} and \tilde{C} , is a function of μ_m and ε_m . In order to properly formulate the problem in a way that is compatible with optimization algorithms, we need express the μ_m and ε_m as frequency-dependent functions, which depend only on a discrete set of parameters. Assuming that the ferrite behaves as a linear, homogeneous, and isotropic material, the effective permittivity can be expressed as [27]

$$\varepsilon(\omega) = \varepsilon_{m,r}\varepsilon_0 - j\frac{\sigma_m}{\omega} \quad (34)$$

where we have assumed that, in this range of frequencies, the contribution from polarization current is a real constant. We have also included the electric conductivity σ_m to allow for the possibility of conduction currents. On the other hand, the complex permeability can be expressed as

$$\mu_m(\omega) = 1 + \chi_m(\omega) = 1 + \chi'_m(\omega) - j\chi''_m(\omega) \quad (35)$$

with χ_m being the magnetic susceptibility. The frequency dependence in ferrite materials is commonly attributed to two mechanisms: natural spin resonance ($\chi_{m,s}$) and domain-wall relaxation ($\chi_{m,d}$) [7]. Hence, the real and imaginary parts of the permeability spectrum can be expressed as

$$\mu'_m(\omega) = 1 + \chi'_{m,s}(\omega) + \chi'_{m,d}(\omega) \quad (36)$$

$$\mu''_m(\omega) = \chi''_{m,s}(\omega) + \chi''_{m,d}(\omega) \quad (37)$$

with

$$\chi'_{m,s}(\omega) = \frac{K_s\omega_s^2[\omega_s^2 + \omega^2(1 + \alpha^2)]}{[\omega_s^2 - \omega^2(1 + \alpha^2)]^2 + 4\omega^2\omega_s^2\alpha^2} \quad (38)$$

$$\chi''_{m,s}(\omega) = \frac{K_s\omega\omega_s\alpha[\omega_s^2 + \omega^2(1 + \alpha^2)]}{[\omega_s^2 - \omega^2(1 + \alpha^2)]^2 + 4\omega^2\omega_s^2\alpha^2} \quad (39)$$

and

$$\chi'_{m,d}(\omega) = \frac{K_d\omega_d^2(\omega_d^2 - \omega^2)}{(\omega_d^2 - \omega^2)^2 + \beta^2\omega^2} \quad (40)$$

$$\chi''_{m,d}(\omega) = \frac{K_d\omega_d^2\beta\omega}{(\omega_d^2 - \omega^2)^2 + \beta^2\omega^2} \quad (41)$$

where K_s is the static spin susceptibility, K_d is the static susceptibility of the domain wall motion, ω_s is the spin resonance angular frequency, ω_d is the domain wall resonance angular frequency, and α and β are damping factors of the domain wall and spin motions. We can also note that K_s and K_m are constrained by the permeability value in the static limit

$$\mu_{m,st} = \lim_{\omega \rightarrow 0} \mu_m(\omega) = 1 + K_s + K_m. \quad (42)$$

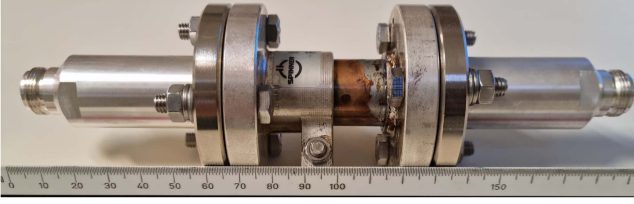


Fig. 6. Coaxial line experimental setup developed for the characterization of ferrite material.

Consequently, the problem reduces to finding the parameters $\mathbb{P} = \{\varepsilon_{m,r}, \sigma_m, K_s, \omega_s, \alpha, K_d, \omega_d, \beta\}$, which provide a better fit between the reference measurement and the model. As these parameters have numerical values with different orders of magnitude, e.g., the quotient $\varepsilon_{m,r}/\omega_s$ varies from 10^{-3} to 10^{-6} , a scaling factor of 10^{-6} was applied to ω_d , ω_s , and β . The fitting procedure is carried out using a *basin-hopping* global optimization method [28] included in the Python scientific package *SciPy* [29] to minimize the following error metric:

$$\frac{1}{N} \sum_n \left| |Z|_{\text{measurements, dB}}(f_n) - |Z|_{\text{TL, dB}}(f_n; \mathbb{P}) \right| \quad (43)$$

where $|Z|_{\text{measurements, dB}}(f_n)$ and $|Z|_{\text{TL, dB}}(f_n)$ are the impedances at frequency f_n , expressed in decibels, obtained from measurements and the TL model, respectively. The algorithm operates by applying a perturbation T of configurable size, $T = 10$ in our case, to the scaled parameters \mathbb{P} followed by a local minimization of $|Z|_{\text{TL, dB}}$. The initial values used were the same for the different cases studied, except for the parameters that were removed from the specific case. The algorithm iterates until a stable minimum is found having as stopping criteria that the global minimum remains the same for a certain number of iterations, which was set to 20 in our case. Additionally, to explore the influence of permittivity and conductivity, we carried out three types of fitting: with permeability only, including $\varepsilon_{m,r}$ with no conductivity, and including both $\varepsilon_{m,r}$ and σ_m . In all cases, the constraint (42) was used to reduce the search space.

1) *MnZn CM Choke in Coaxial Setup*: To measure the CM choke impedance, we designed and built the coaxial line fixture shown in Fig. 6, which fits well the assumptions made to derive the input impedance in Section II. The fixture was made with a 50Ω coaxial line made of copper, with an internal radius $r_i = 4.35$ mm, external radius of $r_o = 10$ mm, and length $l = 215$ mm. The line was terminated with two 7/8" flanges commercialized by Spinner; one of the flanges was soldered to the line, while the other can be opened to introduce the device under test. One of the flanges is a 50Ω port connected to a Rohde & Schwarz ZNL6 vector network analyzer (VNA); the other flange was terminated in a short. The fixture was loaded with a 7427729 toroidal ferrite [10] with dimensions $l_m = 28.5$ mm, $r_i = 4.75$ mm, and $d_m = 4$ mm as labeled in Fig. 1. The ferrite loaded in the coaxial fixture is equivalent to a single turn inductor.

In Fig. 7, we show the magnitude of the impedance reported in the datasheet for this ferrite and the experimental data obtained without setup. We can observe that the datasheet and

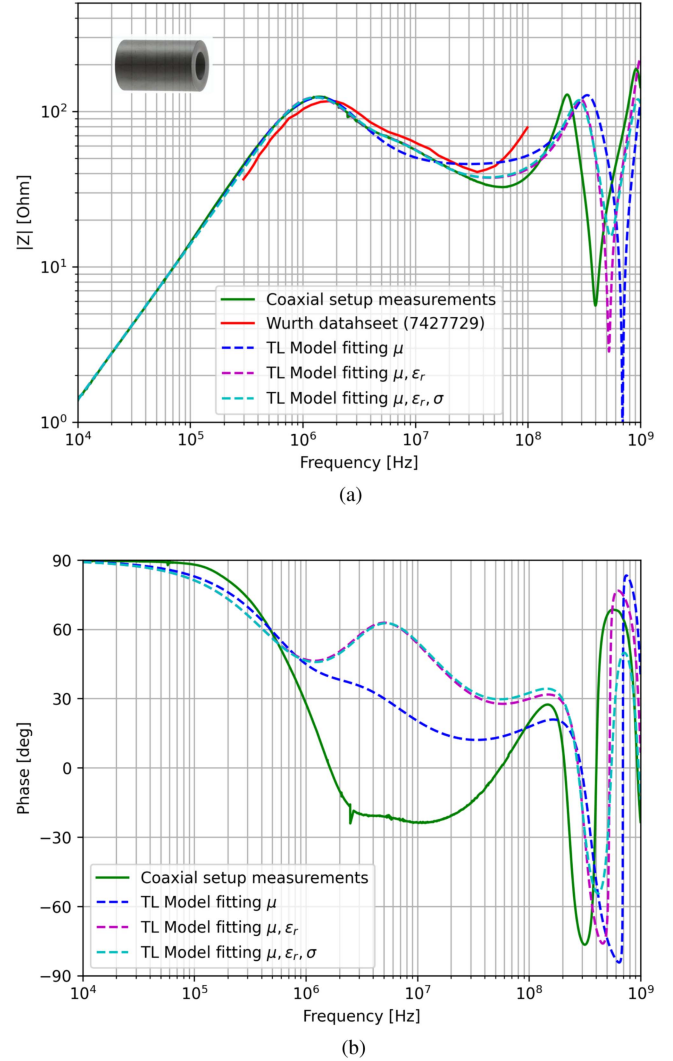


Fig. 7. Plot of experimental measurements of the Wurth 7 427 729 ferrite in coaxial setup (green) which were the target of the fitting procedure. Results for the fittings permeability parameters with vacuum permittivity (blue), with dielectric permittivity (magenta), and with a conductor (cyan). The manufacturer data (red) is shown for comparison. The observed differences low frequency differences are attributed to differences in the sample ($\pm 25\%$ tolerance is expected). The differences above 50 MHz are likely to be produced by differences in the experimental setup. (a) Magnitude. (b) Phase.

our measurements present a good match below approximately 40 MHz and diverge above that value. We attribute this discrepancy to differences in the measurement setup, for which our setup presented a lower parasitic self-inductance. Besides that difference, our sample seems to have a larger permeability at low frequencies, which due to Snoek's law implies also a lower resonant frequency. It is also worth noting (see Fig. 11) that the measured values for the low-frequency permeability diverge significantly and are inconsistent with the value of $\mu_{st,r} = 5000$, which is reported in the datasheet. Using our experimental data as a target for the fitting, we allowed for different parameter searches: with a free-space permittivity ($\varepsilon_{m,r} = 1$, $\sigma_m = 0$), a nonconductive dielectric ($\sigma_m = 0$), and a conductor. The obtained material parameters are reported in Table I; these, together with the fixture and choke dimensions were input in (3)

TABLE I
 MATERIAL PARAMETERS RESULTING FROM THE PARAMETER EXTRACTION PROCEDURE

	$\varepsilon_{m,r}$	σ_m	K_s	ω_s	α	K_d	ω_d	β
7 427 729- μ only	-	-	3845	7.203	1.521	2615	9.501	16.40
7 427 729- $\mu, \varepsilon_{m,r}$	858.0	-	227	82.79	1.528	6233	7.766	15.52
7 427 729- $\mu, \varepsilon_{m,r}, \sigma_m$	1.23	0.22	221	86.76	1.581	6239	7.905	15.87
7 4270 191- μ only	-	-	462	1352	17.26	68	657	1528
7 4270 191- $\mu, \varepsilon_{m,r}$	36.95	-	65	3342	9.335	465	317	1485
7 4270 191- $\mu, \varepsilon_{m,r}, \sigma_m$	1.003	0.0002	463	1320	17.36	67	655	1527

$\varepsilon_{m,r}, K_s, K_m$, and α are a dimensional quantities, ω_s, ω_d , and β are expressed in Mrad/s; σ_m is expressed in S/m. Hyphens stand for values, which were fixed and during the procedure: $\varepsilon_{m,r}=1$ and $\sigma_m=0$.

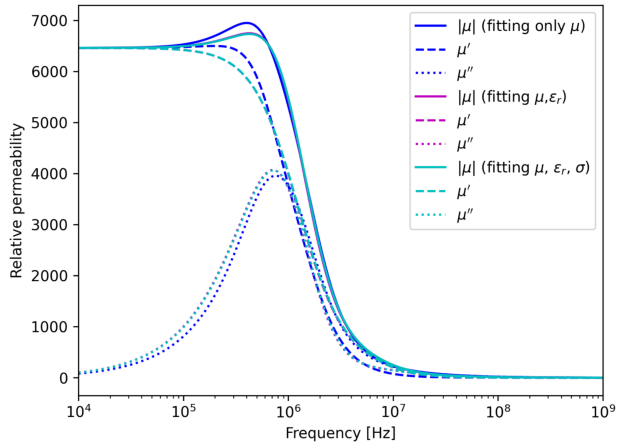


Fig. 8. Permeabilities obtained from the different fittings: Vacuum permittivity (blue), with dielectric permittivity (magenta), and with a conductor (cyan). The fittings for dielectric and conductive-type effective permittivities are overlapped.

to predict the impedances shown in the figure. For the magnitude, we can observe that the best fittings occurred for the two latter cases, which produced very similar results and with a very good match in magnitude with respect to the experimental data up to approximately 30 MHz. Above that frequency, the CM choke impedance is comparable to the one presented by the empty experimental setup, which is close to its self-resonance. While our model is able to qualitatively predict the existence of these resonances, it fails to reproduce the exact place in which they happen. Phase fittings did not produce good results with any of the tested models in the region between 1 and 100 MHz, giving qualitatively good results in the rest of the spectrum. A possible cause is that the permeability models used have only a very small set of values in which they present negative values of permeability; as the optimization algorithm is trying to fit only magnitude, a good fitting of the phase would have been a secondary effect. The permeabilities obtained with the different approaches are shown in Fig. 8, as can be observed, the fittings including permittivity or conductor properties produced very similar results for permeability. For the cases that included effective permittivity, we observe (see Table I) that even a moderate value of σ_m of 0.221 S/m, has a very important effect in the optimal $\varepsilon_{m,r}$, going from ~ 857 to ~ 1 . This high variability can be interpreted as that the setup is not adequate to determine permittivity and highlights that the impedance spectrum is dominated by the permeability values.

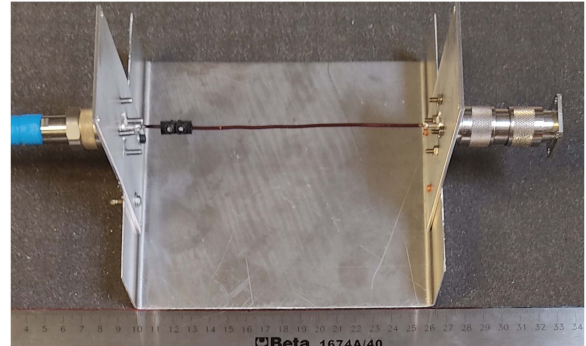


Fig. 9. U-shaped fixture used for the impedance measurement of NiZn chokes (Würth 74 270 191).

2) *NiZn in U-Shaped Fixture*: In this case, we applied the same method to an NiZn ferrite choke (Würth 74270191) with significantly larger dimensions: $l_m = 20$ mm, $r_i = 17.75$ mm, and $d_m = 12.75$ mm (see Fig. 1). This dimensions make it impossible to fit the sample into the previous coaxial fixture. For this reason, we designed and built the U-shaped fixture depicted in Fig. 9. This fixture was made with a bent aluminum sheet, which formed a ground plane with a length of 160 mm at the base, the ports were elevated 50 mm from the base, this distance was use as the external radius r_e as an approximation to the formulas described in Section II. The left port was connected to the same VNA described in the previous setup, and the other was shorted; their live terminals were connected using a copper wire with an internal radius of $r_i = 0.4$ mm. To allow the introduction of the choke, the wire was cut at approximately 20 mm of the left port, and reattached using a removable splice tab.

Before performing measurements with the ferrite, measurements of the unloaded fixture were carried out in order to calibrate the effect of the setup. These measurements were replicated using the same formulas of the proposed model for an empty coaxial line terminated in a short and introducing a shunt-C, series-L network between the feeding port and the line with values $C = 2$ pF and $L = 5$ nH, respectively; a similar procedure as the one carried out in [30]. After calibration, the CM choke was situated in the midpoint of the wire, centered in place using a styrofoam filler with a dielectric characteristic, which was considered negligible. Fig. 10 shows the impedance values measured with this setup, together with the data reported in the Würth datasheet [10]. Contrary to the previous case, the values reported in the datasheet and the ones that we measured differ significantly and while the HF differences could

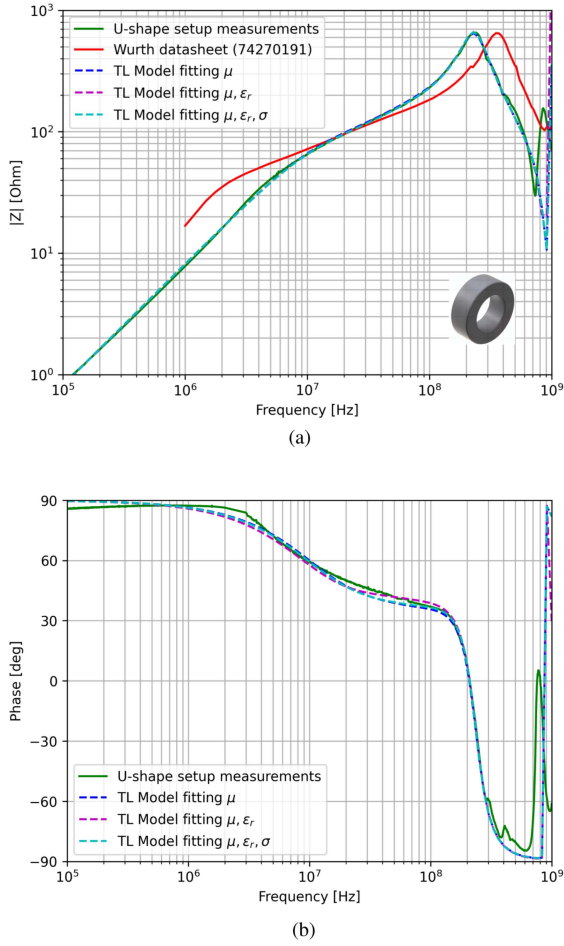


Fig. 10. Plot of experimental measurements of the Wurth 74270191 ferrite in coaxial setup (green) used as a target for the fittings. Results for the fitted permeability parameters with vacuum permittivity (blue), with dielectric permittivity (magenta), and with a conductor (cyan). The manufacturer data (red) are shown for comparison. We observe significant differences at low frequency, which fall out of the tolerance declared by the manufacturer ($\pm 25\%$). The different position of the peak is attributed to a combination of different permeability of the sample and differences in the experimental setup. (a) Magnitude. (b) Phase.

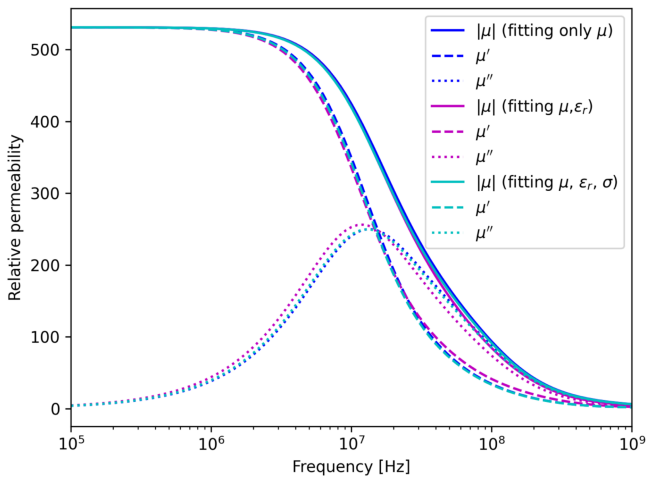


Fig. 11. Permeabilities obtained from the different fittings: Vacuum permittivity (blue), with dielectric permittivity (magenta), and with a conductor (cyan). The fittings for dielectric and conductive-type effective permittivities are overlapped.

be attributed to the experimental setup, the low-frequency ones are possibly caused by differences in the measured samples. With respect to the TL model impedance, the values shown were obtained following the same procedure as in the previous case obtaining very good agreements in magnitude and phase between all models and the measured impedance. Fig. 11 shows the permeabilities obtained with the different models, and the parameters obtained are shown in Table I.

IV. CONCLUSION

A new model for calculating CM ferrite chokes impedance has been developed. The proposed model utilizes the TL theory taking into account the physical size, the measurement setup, and field inhomogeneity. The model's validity was confirmed through simulations and datasheets. It has been shown that by treating the ferrite as a distributed component and incorporating the impedance of the measurement setup, the variation in impedance can be precisely explained. As an application, the model was used to characterize the complex permeability of two ferrites (MnZn and NiZn) operating at different frequency regimes. Due to the geometrical and physical assumptions made, the model is valid only for a single turn of wire. An approach to the modeling of chokes with multiple turns would require to introduce the mutual inductance between the turns into the TL equations, which would result into a set of *delay differential equations*; a task which remains pending for future work.

ACKNOWLEDGMENT

The authors would like to thank the National Institute of Aerospace Technology (INTA) for providing us with the experimental facilities to conduct the measurements used in this article. They also want to thank Würth Elektronik for providing the CM ferrite chokes and Rohde & Schwarz España, S.A. for the ZNL6 VNA used in the experimental measurements.

REFERENCES

- [1] C. R. Paul, *Introduction to Electromagnetic Compatibility*. Hoboken, NJ, USA: Wiley, 2006.
- [2] C. Riener et al., "Broadband modeling and simulation strategy for conducted emissions of power electronic systems up to 400 MHz," *Electronics*, vol. 11, no. 24, 2022, Art. no. 4217. [Online]. Available: <https://www.mdpi.com/2079-9292/11/24/4217>
- [3] A. Nabih, F. Jin, R. Gadelrab, F. C. Lee, and Q. Li, "Characterization and mitigation of dimensional effects on core loss in high-power high-frequency converters," *IEEE Trans. Power Electron.*, vol. 38, no. 11, pp. 14017–14036, Nov. 2023.
- [4] G. Skutt and F. Lee, "Characterization of dimensional effects in ferrite-core magnetic devices," in *Proc. 27th Annu. IEEE Power Electron. Specialists Conf.*, 1996, pp. 1435–1440.
- [5] G. Skutt, "High-frequency dimensional effects in ferrite-core magnetic devices," Ph.D. dissertation, Faculty of the Virginia Polytechnic Institute, Blacksburg, VA, USA, 1996. [Online]. Available: <https://www.proquest.com/docview/304318952?fromopenview=true&pq-origsite=gscholar&parentSessionId=UvLYVDZRvfjUP%2BPw7t4%2Fojd%2FGwxepTuWbUhr0IYxHw%3D>
- [6] F. G. Brockman, P. H. Dowling, and W. G. Steneck, "Dimensional effects resulting from a high dielectric constant found in a ferromagnetic ferrite," *Phys. Rev.*, vol. 77, pp. 85–93, Jan. 1950, doi: [10.1103/PhysRev.77.85](https://doi.org/10.1103/PhysRev.77.85).
- [7] T. Tsutaoka, "Frequency dispersion of complex permeability in Mn-Zn and Ni-Zn spinel ferrites and their composite materials," *J. Appl. Phys.*, vol. 93, no. 5, pp. 2789–2796, 2003.

- [8] J. Eco and A. Limjoco, "Ferrite bead demystified," Application Note AN-1368, 2016, Accessed: Mar. 17, 2023. [Online]. Available: <http://www.analog.com/media/en/technical-documentation/application-notes/AN-1368.pdf>
- [9] B. Anicin, D. Davidovic, P. Karanovic, V. Miljevic, and V. Radojevic, "Circuit properties of coils," *IEE Proc.-Sci., Meas. Technol.*, vol. 144, no. 5, pp. 234–239, 1997.
- [10] W. E. eiSos GmbH, "Datasheet WE-Fi leaded toroidal line choke," Würth Elektronik, Tech. Rep. 7427729, 2020. [Online]. Available: <https://www.we-online.com/components/products/datasheet/7427729.pdf>
- [11] A. Payne, *Self-Resonance in Air Coils*. London, U.K.: Alan Payne Associates, 2021.
- [12] M. Kazimierczuk, G. Sancineto, G. Grandi, U. Reggiani, and A. Massarini, "High-frequency small-signal model of ferrite core inductors," *IEEE Trans. Magn.*, vol. 35, no. 5, pp. 4185–4191, Sep. 1999.
- [13] S. D. Mitchell and J. S. Welsh, "The influence of complex permeability on the broadband frequency response of a power transformer," *IEEE Trans. Power Del.*, vol. 25, no. 2, pp. 803–813, Apr. 2010.
- [14] E. S. Lee and B. G. Choi, "Calculation methodologies of complex permeability for various magnetic materials," *Electronics*, vol. 10, no. 17, 2021, Art. no. 2167.
- [15] M. K. Ghosh et al., "Numerical modelling of magnetic characteristics of ferrite core taking account of both eddy current and displacement current," *Heliyon*, vol. 5, no. 8, 2019, Art. no. e02229.
- [16] A. Suarez et al., "Characterization of different cable ferrite materials to reduce the electromagnetic noise in the 2–150 kHz frequency range," *Materials*, vol. 11, no. 2, 2018, Art. no. 174.
- [17] M. Kacki, M. S. Rylko, J. G. Hayes, and C. R. Sullivan, "Analysis and experimental investigation of high-frequency magnetic flux distribution in Mn-Zn ferrite cores," *IEEE Trans. Power Electron.*, vol. 38, no. 1, pp. 703–716, Jan. 2023.
- [18] T. Tsutaoka, T. Nakamura, and K. Hatakeyama, "Magnetic field effect on the complex permeability spectra in a Ni-Zn ferrite," *J. Appl. Phys.*, vol. 82, no. 6, pp. 3068–3071, 1997.
- [19] T. Tsutaoka, T. Kasagi, and K. Hatakeyama, "Magnetic field effect on the complex permeability for a Mn-Zn ferrite and its composite materials," *J. Eur. Ceram. Soc.*, vol. 19, no. 6, pp. 1531–1535, 1999.
- [20] T. P. Todorova, A. V. D. Bossche, and V. C. Valchev, "A procedure for the extraction of intrinsic AC conductivity and dielectric constant of N87 Mn-Zn ferrite samples based on impedance measurements and equivalent electrical circuit modeling," *IEEE Trans. Power Electron.*, vol. 33, no. 12, pp. 10723–10735, Dec. 2018.
- [21] S. Yamada, E. Otsuki, and T. Otsuka, "AC resistivity of Mn-Zn ferrites," in *Proc. 13th Int. Telecommun. Energy Conf.*, 1991, pp. 703–708.
- [22] S. Yamada and E. Otsuki, "Analysis of Eddy current loss in Mn-Zn ferrites for power supplies," *IEEE Trans. Magn.*, vol. 31, no. 6, pp. 4062–4064, Nov. 1995.
- [23] D. Pozar, *Microwave Engineering* (Electrical and Computer Engineering). Hoboken, NJ, USA: Wiley, 2012.
- [24] K. Namjoshi, J. D. Lavers, and P. Biringer, "Eddy-current power loss in toroidal cores with rectangular cross section," *IEEE Trans. Magn.*, vol. 34, no. 3, pp. 636–641, May 1998.
- [25] R. L. Stoll, *The Analysis of Eddy Currents*. Oxford, U.K.: Clarendon, 1974.
- [26] A. Stadler, M. Albach, and A. Lindner, "A practical method to measure electrical AC conductivity of MnZn ferrites using conventional toroids," *IEEE Trans. Magn.*, vol. 46, no. 2, pp. 678–681, Feb. 2010.
- [27] R. C. Rumpf, *Electromagn. and Photon. Simul. for the Beginner: Finite-Difference Freq.-Domain in MATLAB*. Boston, MA, USA: Artech House, 2022. [Online]. Available: <https://empossible.net/fdfdbook/>
- [28] D. J. Wales and J. P. Doye, "Global optimization by basin-hopping and the lowest energy structures of Lennard-Jones clusters containing up to 110 atoms," *J. Phys. Chem. A*, vol. 101, no. 28, pp. 5111–5116, 1997.
- [29] P. Virtanen et al., "SciPy 1.0: Fundamental algorithms for scientific computing in Python," *Nature Methods*, vol. 17, pp. 261–272, 2020.
- [30] D. Stepins, G. Asmanis, and A. Asmanis, "Measuring capacitor parameters using vector network analyzers," *Electronics*, vol. 18, no. 1, pp. 29–38, 2014.



Alejandro Muñoz Manterola received the M.Sc. degree in material science from the University of Oviedo, Oviedo, Spain, in 2019. He is currently working toward the Ph.D. degree in computational electromagnetism with the University of Granada, Granada, Spain.

His current research includes computational electromagnetics, electromagnetic compatibility, and material analysis.

Mr. Manterola was the recipient of the FPI Scholarship,



Luis Manuel Díaz Angulo (Member, IEEE) received the M.Sc. and Ph.D. degrees in physics and the M.Sc. degree in electronics engineering from the University of Granada, Granada, Spain, in 2008, 2014, and 2015, respectively.

He is currently an Associate Professor with the Department of Electromagnetism and State Matter, University of Granada, Granada, Spain. He has worked in time domain computational electromagnetics, especially discontinuous Galerkin and finite-differences. The main applications of these methods have been in the areas of electromagnetic compatibility, and material characterization.



Alberto Gascón Bravo received the M.Sc. and Ph.D. degrees in physics from the University of Granada, Granada, Spain, in 2009 and 2014, respectively.

He is currently a postdoc with the Department of Electromagnetism and Matter Physics, University of Granada. He has worked in the fields of astroparticle physics and accelerator physics. His current research interests include electromagnetic compatibility, computational electromagnetism and material analysis.



Kenan Tekbaş received the M.Sc. degree in communication engineering and the Ph.D. degree in electrical and electronic engineering from The University of Manchester, Manchester, U.K., in 2012 and 2017, respectively.

He is currently a Postdoctoral Marie Skłodowska-Curie Fellow with the Department of Electromagnetism, University of Granada, Granada, Spain. His research interests include computational electromagnetics, the finite-difference time-domain methods, electromagnetic compatibility, magnetic materials, bioelectromagnetism, and high-performance computing.



María Tijero received the Ph.D. degree in communications, electronics & control from the University of the Basque Country (UPV/EHU), Leioa, Spain, in 2007.

She is currently an Industrial Engineer with the ETS Industrial Engineering and Telecommunications of Bilbao (UPV/EHU), in 2001. She has been a Researcher with Ikerlan, Gipuzkoa, Spain, since 2007. She was with the EMC Laboratory (Electro Magnetic Compatibility), working for the health, automotive, industrial, and railway sectors. Her present research interest is 3D-FEM simulation of electromagnetic effects in electronic systems.



Roberto Moreno was born in Eibar, Spain, in 1974. He received the B.S. degree in electronic engineering from Mondragon Unibertsitatea, Mondragón, Spain, in 1998.

Since 1998, he has been with the Department of Electronics (now Hardware Systems and Communications Area), Ikerlan Research Center, Mondragón, Spain. Since 2008, he has been the head of EMC and nonfunctional requirements laboratory and Researcher. His current research interests include electrical and electronic behavior analysis and simulation

of power and control electronics in the EMC area.



Salvador G. García (Senior Member, IEEE) received the M.Sc. and Ph.D. degrees (with extraordinary award) in physics from the University of Granada, Granada, Spain, in 1989 and 1994, respectively.

He is currently a Full Professor with the Department of Electromagnetism and Matter Physics, University of Granada. He has authored or coauthored 90 refereed journal articles and book chapters and led several national and international projects. In 2010 he cofounded the startup Elemwave devoted to numerical solver development and EM consultancy. His current research interests

include computational electromagnetics, electromagnetic compatibility, RCS, antenna design, and material analysis.